The efficiency of secondary organic aerosol particles to act as ice nucleating particles at mixed-phase cloud conditions

Wiebke Frey[1], Dawei Hu[1], James Dorsey[1], M. Rami Alfarra[1,2], Aki Pajunoja[3], Annele Virtanen[3], Paul Connolly[1], and Gordon McFiggans[1]

[1]Centre for Atmospheric Science, School of Earth and Environmental Sciences, The University of Manchester, Manchester, UK
[2]National Centre for Atmospheric Science (NCAS), The University of Manchester, Manchester, UK
[3]Department of Applied Physics, University of Eastern Finland, Kuopio, Finland

Correspondence to: Wiebke Frey (wiebke.frey@manchester.ac.uk)

Abstract. Secondary Organic Aerosol (SOA) particles have been found to be efficient ice nucleating particles under the cold conditions of (tropical) upper tropospheric cirrus clouds. Whether they also are efficient at initiating freezing at slightly warmer conditions as found in mixed phase clouds remains undetermined. Here, we study the ice nucleating ability of photo-chemically produced SOA particles with the combination of the Manchester Aerosol and Ice Cloud Chambers. Three SOA systems were

5 tested resembling biogenic/anthropogenic particles and particles of different phase state. After the aerosol particles were formed, they were transferred into the cloud chamber where subsequent quasi-adiabatic cloud evacuations were performed. Additionally, the ice forming abilities of ammonium sulfate and kaolinite were investigated as a reference to test the experimental setup.

Clouds were formed in the temperature range of -20°C to -28.6°C. Only the reference experiment using dust particles showed

10 evidence of ice nucleation. No ice particles were observed in any other experiment. Thus, we conclude that SOA particles produced under the conditions of the reported experiments are not efficient ice nucleating particles starting at liquid saturation under mixed-phase cloud conditions.

1 Introduction

Clouds and their feedbacks are major sources of uncertainty in future climate predictions. Aerosol particles to a significant

15 extent determine the condensation of water to form liquid droplets and ice crystals. The transition into the ice phase is particularly important, e.g. for formation of precipitation, but is yet poorly understood in detail. While certain aerosol particles such as dust are known to be important ice nucleating particles (INP), others are highly abundant, yet their ice forming abilities remain poorly understood. One example for such particles are secondary organic aerosol (SOA). They originate from biogenic and anthropogenic sources, e.g. from the oxidation of plant, biomass burning, and combustion emissions. SOA particles can

20 exist in different phase states. The traditional understanding conceived them as homogeneous well-mixed liquids but they can occur in amorphous semi-solid or solid states (Virtanen et al., 2010). The state of the particles is dependent on the relative humidity and temperature (Koop et al., 2011). Amorphous solid, also termed glassy, particles have been observed to bounce in

an aerosol impactor, thus, the bounce of particles can be used to infer their phase state (Virtanen et al., 2010). The amorphous phase state of these glassy particles has been shown to influence their ability to act as ice nucleating particles. For example Murray et al. (2010) have found glassy organic particles to be efficient ice nucleating particles in the depositional mode in the tropical tropopause layer. In their experiments, Murray et al. (2010) found that glassy aerosol particles nucleated ice crystals at

5   lower relative humidities (with respect to ice) than the same aerosol in a non-glassy phase state. Furthermore, fewer particles nucleated on the glassy particles, allowing higher in-cloud humidities. Shiraiwa et al. (2017) state that in the middle and upper troposphere SOA should be mostly in the glassy state, which may promote ice nucleation. They found SOA to undergo their glass transition above 2km altitude. Similarly, Mikhailov et al. (2009) state that a moisture-induced glass transition may play a role in the lower troposphere, depending on the relative humidity.

10 Several studies have investigated the ice forming capability of different SOA particles; however, the majority of these studies looked at cirrus temperatures (i.e. below -40°C) and only few investigations look at the temperature range of mixed-phase clouds. One example of such a study is reported by Prenni et al. (2009). They looked at the ice nucleating ability of alkenes at -30°C and found them to be unlikely to participate in heterogeneous nucleation. However, they formed the SOA particles by dark ozonolysis of precursors. To our knowledge, the efficiency of photo-chemically produced SOA particles as ice nucleating

15 particles has not been determined.

The freezing and eventual sublimation of ice from the aerosol particle may change its properties (e.g. Adler et al., 2014): so called cloud processing. Thus, such a freeze-drying cycle might increase their ice nucleating abilities. Cloud processing also happens in warm clouds (e.g. Hoose et al., 2008), where the aerosol particle characteristics can be changed e.g through additional uptake of atmospheric gases and chemical reactions with the soluble part of the contained aerosol particle take place in

20 the aqueous phase. Upon evaporation of the cloud, aerosol particles are re-emitted and these particles have changed chemical properties and are larger than the initial particles (Pruppacher and Klett, 1997); therefore, the aerosol size distribution is also affected by cloud processing. Comparison of size distribution of interstitial aerosol within the cloud with the size distribution below the cloud clearly indicates that the processing of the aerosol through (nonprecipitating) stratus can lead to increased mass of the subset of particles which had served as cloud condensation nuclei (CCN; Hoppel et al., 1994).

25 This work aims to investigate the ice nucleating ability of photo-chemically produced SOA particles in the Manchester Aerosol and Ice Cloud Chambers. Here, we report on the results of the measurements (Sect. 3, including the experimental setup), after an introduction of the chambers and instrumentation (Sect. 2). The results are discussed in relation to previous studies and their impact for atmospheric processes (Sect. 4) and summarised in the conclusions (Sect. 5).

2   Facilities and Instrumentation

30 For the current study the Manchester Ice Cloud Chamber (MICC) and Manchester Aerosol Chamber (MAC) were used, which are connected by a transfer pipe. The chambers and their instrumentation are described in the following, an overview is given in Fig. 1.

2.1 Manchester Aerosol Chamber (MAC)

The Manchester Aerosol Chamber (MAC) is a photochemical aerosol chamber comprising a $18m^3$ teflon bag (Hamilton et al., 2011; Alfarra et al., 2013) surrounded by a temperature and relative humidity controlled housing. The teflon bag is held by three frames such that the upper and lower frame can freely move to allow expansion and collapsing of the chamber during fill

5   cycles or sampling (and thus removing air) from the chamber. Attached to the chamber is an air system that contains a series of filters (Purafil, Purafil Inc., USA; charcoal; HEPA, Donaldson Filtration, USA), a humidifier, an ozoniser, and a seed drum. NO_x can be added (as NO_2) as well as the target volatile organic compounds (VOCs) for SOA formation. The precursors are introduced through injection into a heated glass bulb and transferred into the chamber by a flow of filtered, high purity nitrogen (ECD grade, 99.997 %). Thus, the composition of gaseous precursors and relative humidity can be controlled. Two 6kW Xenon

10   arc lamps and further halogen bulbs are mounted on the inside of the bag's housing to simulate the solar spectrum and enable photo-chemistry. Furthermore, the housing is covered with reflective space blanket, in order to maximise the irradiance in the bag and to ensure even illumination. The Xenon arc lamps are mounted on two opposite sides of the enclosure at different heights. The illumination setup has been tuned to mimic the atmospheric actinic spectrum over the wavelength range 290–800nm. Air conditioning ensures that the chamber is kept at an operating temperature of typically 25°C during experiments

15   (under illumination). Further details on the chamber and illumination can be found in Alfarra et al. (2013).

The aerosol chamber is equipped with a set of instruments to measure temperature, humidity, aerosol number, particle size distribution, mass concentration and chemical composition. Relative humidity and temperature are measured at the centre and on the side of the chamber by a dewpoint hygrometer, a thermocouple, and a resistance probe. A water condensation particle counter (WCPC 3785, TSI Inc., USA; with a cut-off diameter at 5 nm nm) is used to measure the aerosol number

20   concentrations. A Differential Mobility Particle Sizer (DMPS, custom made) observes particle size and mass distributions for sizes between 40–640nm with the sheeth flow taken from the chamber as well. A chemiluminescence gas analyser (Model 42i, Thermo Scientific, USA) is used for measuring NO and NO_2 mixing ratios and ozone was measured by a UV photometric gas detector (Model 49C, Thermo Scientific, USA).

A transfer pipe connects the aerosol chamber to the cloud chamber (as indicated in Fig. 1). The pipe has a diameter of one inch

25   and is approximately 33m long.

2.2 Manchester Ice Cloud Chamber (MICC)

The Manchester Ice Cloud Chamber (MICC) is a 10m high stainless steel tube of 1m diameter which is contained in three cold rooms (spanning over three floors; Connolly et al., 2012; Emersic et al., 2015). The cold rooms can be temperature controlled from room temperature to about -50°C. Two scroll pumps are used to evacuate the chamber in order to form clouds in these

30   experiments. The chamber can be refilled e.g. with filtered air or air from the aerosol chamber via the transfer pipe (cf. Fig. 1). MICC is instrumented to measure ambient conditions such as temperature, pressure, and humidity, and furthermore, cloud particle and aerosol particle concentrations. The following instruments are in use: eight thermocouples (K type) at different heights, reaching alternating 10cm (thermocouples Tc1, Tc3, Tc5, Tc7) or 50cm (thermocouples Tc2, Tc4, Tc6, Tc8) into the

chamber. The thermocouples were calibrated before the experiments at temperatures between -78.5°C (dry ice) and 100°C (boiling point). The thermocouples have a time constant of about 60s, see appendix for more detail. A modified (for lower temperatures) Keller Lex1 pressure sensor with accuracy of 0.2%FS monitors the chamber pressure. Humidity can be measured at ambient pressure by a CR-4 hygrometer. For the measurements of cloud particle properties such as number concentrations,

5 size distributions, and shapes, a Forward Scattering Spectrometer Probe (FSSP Dye and Baumgardner, 1984) and a Cloud Particle Imager (CPI, version 1.0; Connolly et al., 2007) were deployed.

2.3 Cleaning procedures

In order to clean the chambers the attached air system accommodates three filters (see description in Sect. 2.1 and Fig. 1) to remove any particles and reactive gases.

10 The aerosol chamber is cleaned by several cycles of filling and flushing (at least 5 times) until the aerosol number concentrations stayed constant below 5cm^{-3} (dark concentration). The cleaning procedure includes flushing the pipes around the seed drum and ozoniser. After the last flushing cycle ozone is added into the chamber and left over night in order to oxidise any left-over reactants. Typically for this purpose, ozone concentrations are about 500-600ppb. The content of the chamber is then replaced with clean air using a series of fill/flush cycles prior to the experiment.

15 The cloud chamber is cleaned by repeated evacuations of the chamber to 200hPa followed by refilling from the air system with filtered air until aerosol concentrations stayed constant below 1cm^{-3}. The number of necessary cleaning cycles is dependent on the aerosol number concentrations left from a previous experiment.

As the cloud chamber is fitted with several outlets/openings, which for evacuation are sealed off, there are sources for leakages. These have been measured by evacuating the chamber to 200hPa and leaving it at this pressure for approximately two hours.

20 A leakage rate of $0.12\text{hPa}\,\text{min}^{-1}$ was found, which should only allow introduction of a small number of unspecified aerosol from the lab air. An estimate including previous leak checks and concurrent aerosol concentration measurements suggests an introduction of less than 1.5cm^{-3} when leaving the chamber 5 minutes at 200hPa. (Less aerosol is introduced through leakages at higher pressures in the cloud chamber.) The leak check included the transfer pipe, i.e. the valve to the transfer pipe on the cloud chamber side was open and just closed at the entrance to the air system. The refilling of the cloud chamber with air from

25 the aerosol chamber was performed as quickly as possible, to reduce time when MICC and transfer pipe are underpressured and can potentially be contaminated (typically started within 1 minute). A transfer, i.e. the refilling of the cloud chamber from the aerosol chamber to ambient pressure, takes about 10 minutes.

The air system itself is a complex system with various fittings; therefore, it presents a further potential source for contamination during transfers. This was tested by "clean bag" transfers, where both chambers are cleaned and a transfer is performed with

30 (almost) particle free air from the aerosol chamber bag (measurements are shown in supplementary material).

In addition to the cleaning procedures, MICC is regularly defrosted to avoid build-up of ice on the sample line outlets to the cloud particle instrumentation that would eventually lead to particle losses.

3 Experiments

The experimental programme was constructed to test the efficiency of SOA to act as ice nucleating particles at -20°C to around -28°C, i.e. under conditions roughly resembling mixed-phase clouds where dust starts to become important as ice nucleating particle. Three different SOA systems were used to perform the experiments. They were chosen to be representative of a typical range of SOA particles of varying sources found in the atmosphere, including anthropogenic/biogenic as well as particles of different phase state (bouncy/non-bouncy particles; Virtanen et al., 2010). The SOA were photochemically formed from the following precursors: α-pinene (biogenic and bouncy[1]), 1,3,5-trimethylbenzene (TMB; anthropogenic and bouncy[1]), and heptadecane (anthropogenic and non-bouncy[1]). In order to test the experimental setup, the experiments using SOA particles for cloud formation were accompanied with experiments using ammonium sulfate. Ammonium sulfate was chosen as it is a well known system that does not nucleate ice under the chosen experimental conditions. Furthermore, it can easily be tested with a model to assess whether the ammonium sulfate measurements are meaningful (see Sec. 3.3. A further control experiment was performed using dust (kaolinite) as this is known to be an ice nucleating particle at the given temperature. Some systems have been tested with two different pump speeds during evacuation which alters the cooling rate. Cooling rates were about $10.1 \mathrm{K}\,\mathrm{min}^{-1}$ and $6.2 \mathrm{K}\,\mathrm{min}^{-1}$ for fast and slow pump speed, respectively. An overview of the performed experiments is given in Table 1.

3.1 Experimental design

An experiment always followed the outlined procedure: After careful cleaning of the chambers and the air inlet system, the desired particles are created in MAC. To achieve this the volatile organic compound (VOC) injection glass bulb is heated and flushed with nitrogen. During the last filling of the MAC air bag the precursor gases for the SOA and NO_x are injected. By filling through the humidifier water vapour is added. Mixing within the bag is ensured by the main filling air stream. Photochemistry is started by switching on the lights. Ozone is injected as well just after the lights are switched on as a source of OH to speed up aerosol nucleation and to increase particle numbers. After sufficient time for the photochemistry, the lights are switched off and the cloud chamber is evacuated to prepare for the transfer. Table 2 shows the initial concentrations and other chamber conditions used for the formation of SOA particles. A typical development of the formation of a SOA system is shown in Figure 2.

When aerosol particle mass reached equilibrium in MAC, a transfer was performed from MAC to MICC. For the transfer MICC was evacuated to 200hPa and then refilled from MAC to ambient pressure. Thus, the desired aerosol population is transferred into the cloud chamber and slightly diluted by the remaining air in MICC, i.e. approximately $8\mathrm{m}^3$ air from MAC is transferred to MICC and mixed with the approximately $2\mathrm{m}^3$ remaining clean air. The transfer was then followed by measuring aerosol total number concentration and size distribution in MICC (using the CPC and SMPS). Temperatures in MICC fluctuate during a transfer, decreasing during evacuation and increasing during refill, even above the target temperature of 253K, as the aerosol chamber is operated at room temperature, and the transferred air needs time to cool. Therefore, further aerosol

---

[1]see supplement for more information on particle bounce.

measurements were obtained after MICC temperatures settled back to the target temperature. Immediately following these aerosol measurements, a cloud expansion was performed, i.e. MICC was pumped down to 700hPa with the cloud probes sampling from the chamber as well. Two different pump speeds were tested, a faster pump speed using both main pumps and the pumps attached to the cloud probes, and a slower pump speed using one of the main pumps only in addition to the

5   cloud probes. A faster pump speed, assuming adiabaticity, will lead to a faster cooling rate and higher supersaturations. MICC was refilled again from MAC, to avoid further dilution of the aerosol by mixing with filtered air. Again, aerosol number concentrations and size distributions were measured in MICC two times and a further cloud expansion was performed. If there was still enough air remaining in MAC, it was used to refill MICC which allowed a third cloud run.

Additionally, cloud expansions on background transfers were performed. The background experiments normally contain all of

10   the ingredients used in a typical SOA experiment with the exception of the main precursor. They are conducted to quantify the contribution of background VOCs and oxidants to the overall SOA formation and to ensure that the SOA formed during actual experiments is a result of the oxidation of the precursors being studied (i.e. not originating from compounds coming off the chamber walls or from the air used to fill the chamber).

3.2   Results

15   Instead of showing data for all cloud expansions here, we will only illustrate in detail two examples, one using heptadecane as precursor and one α-pinene, as the latter looks fairly similar to the TMB experiment. For the sake of completeness, figures for all other expansions can be found in the supplementary material. An example for a cloud expansion on SOA formed on heptadecane precursor with the faster pump speed is shown in Fig. 3. The uppermost panel shows the aerosol size distribution measured by the SMPS prior to the chamber evacuation, along with the numbers for total aerosol concentration as observed by

20   the SMPS. Agreement of the size distributions observed after transfer and before expansion shows that there is no significant alteration of the aerosol size distribution as a result of the transfer and the time spend in MICC while the temperatures settle. The mean mode diameter of the aerosol is located at about 370nm, while the second mode diameter is at about 200nm. Thus, these aerosol particles are large enough to potentially act as ice nucleating particles. Simultaneously with the aerosol measurements, humidity was scanned in MICC. These observations show that MICC was saturated with respect to water (supersaturated with

25   respect to ice), the dew point was at 252.6K after the transfer and at 252.7K before the expansion. The further panels in Fig. 3 show the time series of the cloud development, with the size distribution and mean volume diameter (MVD) of cloud particles (panel b) observed by the FSSP, total water content (TWC) and number concentration (N; panel c), pressure and temperature (panel d), and some example images taken by the CPI (panel e). Cloud particles observed just at the start of the expansion potentially stem from opening the valve to the instrument inlet and should not be considered.

30   At the beginning of the expansion (first 20 seconds) a small number of aerosol particles (approx. 30cm^{-3}) activate to cloud particles with sizes mostly below 10μm. The main activation takes place at 21 seconds, apparent from the cloud particle size distribution time series. High numbers of small hydrometeors are observed that subsequently grow to slightly larger sizes (cf. yellow colours showing the main particle size mode and superimposed mean volume diameter (MVD, light blue) in the plot). The CPI only detected spherical particles during the expansion. We would expect that potential ice particles would grow to

larger sizes than the observed sizes. Taking the sizes and the imaged spherical shapes into consideration, it can be comfortably assumed that the observed particles were water droplets.

Fig. 4 shows the example of a cloud evacuation run performed with a slow pump speed on α-pinene as SOA precursor. The mean mode diameter of the aerosol is at about 210nm. Activation of aerosol to cloud particles starts at 30s into the cloud run.

5 Particle sizes stay below 20μm, the mean volume diameter reaches about 9μm at about 90 seconds into the evacuation and stays fairly constant until the cloud diminishes. Only one spherical particles had been imaged by the CPI. Given that there was no further growth in particle size and particle sizes are rather small, we conclude that the particles were in the liquid phase and not frozen. In case of frozen particles, we would have expected those to grow more quickly to larger sizes, e.g. as in the dust example below.

10 In order to show that ice can be formed under the experimental conditions, dust particles were injected into the cloud chamber. The kaolinite dust was injected into the cloud chamber with the help of a dust generator (PALAS RBG1000) directly attached to the chamber (not via the air system). To ensure proper mixing of the dust and air in the chamber an evacuation to 700hPa was performed directly after the injection. The results of the dust run using the high pump speed is shown in Fig. 5. Dust particles of a wide range of sizes were present (see SMPS size distribution). At first, small particles with mean volume diameters

15 between 4μm and 10μm were observed that were presumably large (swollen) dust particles. Upon activation at 21 seconds, small particles activated in the droplet mode (cf. yellow colours in the size distribution time series), followed by particle growth and diminishing of the small droplet mode. The drop of cloud particle numbers at about 80s into the evacuation are caused by the growths of the larger ice particles, at the expense of the small droplets (Wegener-Bergeron-Findeisen process). The CPI images show the presence of non-spherical particles, i.e. ice particles.

20 The two successive cloud runs in each experiment can be used to look at activated fractions in order to see whether the aerosol properties change after one activation/deactivation cycle (cloud processing). The activated fraction here is simply calculated by dividing the pre-expansion aerosol number concentration by the peak cloud particle number concentration. Furthermore, when a second experiment is available with a different pump speed, this can be used to determine the effect of the cooling rate on the activation of the aerosol. Fig. 6 shows the activated fractions of five experiments: the already shown heptadecane (upper

25 left panel), α-pinene (middle right panel), and dust (lower right panel) runs accompanied by their 'sister'-runs, plus a further heptadecane experiment with altered pump speed (lower left panel) and a TMB experiment (upper right panel). Instrument error margins may lead to an activated fraction of more than 1. The fast pump speed heptadecane experiment shows no significant cloud processing, activated fractions of both runs are very similar. In the slower pump speed experiment, however, the second heptadecane run shows a higher activated fraction than the first run. Thus, the aerosol becomes more efficient at activating to

30 droplets. The first run here exhibits lower activated fractions as the fast pump speed runs, the second run peak activated fraction is about the same as in the fast pump speed runs. The α-pinene slow pump speed experiment shows the opposite behaviour, the second cloud run has slightly lower activated fractions as the first. The same is true for the TMB slow pump speed runs. Caution needs to be taken with the outliers in the first α-pinene run, which might be due to oversampling in the FSSP. The dust runs were performed at different pump speeds, the second run using the slower pump speed shows slightly lower activated

35 fractions as the fast pump speed run.

3.3 Model comparison for ammonium sulfate control experiment

The Aerosol-Cloud and Precipitation Interactions Model (ACPIM; Connolly et al., 2012) has been chosen for testing of the experimental data of the ammonium sulfate control runs. The model is adapted to be used with chamber measurement data as the ones reported here. The observed temperature and pressure curves as well as the initial relative humidity and aerosol size distribution and number concentrations are used to initialise the model. Figure 7 shows the results of the ACPIM simulation in comparison to the measurements of cloud droplet number concentrations, LWC, and size distribution. The model predicts complete activation of the aerosol particles. The measurements show some outliers which might indicate that the capacity of the instrument for measuring particle numbers has been reached, i.e. too many particles lead to overcounting which is apparent in the outliers. Apart from the outliers, the measured cloud particle numbers are a little smaller than the modelled numbers, again in high concentrations the instrument is prone to measurement coincidence errors, not only overcounting but also multiple particles in the sample volume at one time leading to a general undercounting. As all aerosol particles in ACPIM activate, they grow subsequently into a very narrow (theoretical) size distribution. The simulated sizes are somewhat smaller than the mean volume diameter measured by the FSSP. This could be the reason for the smaller LWC predicted than measured as well. The simulation predicts cloud particle appearance earlier than the observations show, this is certainly due to boundary layer effects in the cloud chamber. Due to e.g. wall heating, the air next to the walls may stay cloud free for longer than the interior of the chamber where the cloud forms earlier on. As the sample lines are attached to the bottom and will first suck air from the boundary layer, it will take time for the cloud to extend downwards to the bottom and be sampled. The observed cloud particle size distribution is wider than the simulated one. Some aerosol particles might nucleate and subsequently activate into cloud drops during the evacuation, leading to the widening of the size distribution to the smaller sizes. Further effects of non-uniformity in temperature and humidity might lead to further broadening of the size distribution. However, the simulation and measurements are similar enough to conclude that the measurements behave reasonably as expected.

4 Discussion

Three different precursors were chosen for SOA formation in this study, to cover biogenic and anthropogenic as well as bouncy and non-bouncy particles. The photo-oxidised SOA particles were transferred into a cloud chamber to study their ice nucleating abilities at temperatures of -20°C to about -28°C. The chamber was at water saturation at the start of the measurements, thus, providing the environment for cloud formation. The most important finding from this study is that the used SOA particles were not efficient ice nucleating particles at the chosen temperature range (i.e. in the mixed phase clouds regime). While the sensitivity runs performed on dust particles, clearly show nucleation of ice, ice nucleation was not measurable in any of the other SOA or ammonium sulfate runs. Thus, even though abundant, SOA particles might not play a role in ice formation at lower altitudes, contrary to previous findings at lower temperatures, where SOA particles were found to nucleate ice (see Hoose and Möhler, 2012, and references therein). Measurements of ice nucleation (or lack of ice nucleation) at higher temperatures are scarce. Prenni et al. (2009) also found no measurable ice nucleation in continuous flow chamber measurements at -30°C, however, they formed the SOA particles through dark ozonolysis of precursors using excessive amounts of ozone, whereas in this study

photo-oxidation of precursors with less ozone were used. Furthermore, the residence time of the aerosol particles in Prenni et al.'s measurements in the continuous flow chamber are in the order of seconds, compared to several minutes here. Even if e.g. Mikhailov et al. (2009) and Shiraiwa et al. (2017) are correct in assuming that glass transition plays a role at ambient temperatures in the lower troposphere (above roughly 2km), these particles according to this study and Prenni et al. (2009) will

5 not be (efficient) ice nucleating particles.

There seems to be a twofold activation of cloud droplets in the heptadecane experiments. Upon onset of activation a few seconds after start of the evacuation, a smaller amount of cloud particles are observed with a low LWC, until the second mode of activation kicks in and larger numbers of particles activate and the LWC peaks. The mean volume diameter of the cloud particles in the first activation mode is a little smaller than in the second mode, though not always clearly apparent. Also in the

10 dust experiments two modes were observed in the size distribution. Here, however, it is likely that the first mode comprises larger (possibly swollen) dust particles and not cloud particles. The latter appear in the second mode. The experiments with α-pinene and TMB precursors show a different behaviour with only the main activation mode. These precursors are both bouncy, i.e. more viscous than the heptadecane. Thus, larger supersaturations are needed for these precursors to take on water vapour and grow due to diffusion limitations. A speculative explanation for this could be that the heptadecane particles, or rather a

15 subset thereof, already start activating during the transfer. The relatively warm air from the aerosol chamber flows into the cold cloud chamber and starts cooling, the relative humidity increases accordingly. Some vapour will condense onto the walls, but the relative humidity might increase enough to start activation of aerosol particles that already made it into the chamber. These activated particles then grow, while further later arriving particles may stay unactivated. When the evacuation of the cloud chamber starts, cooling will be much higher and all other heptadecane particles will activate as well. However, the aerosol

20 chamber DMPS and cloud chamber SMPS aerosol size distributions do not indicate major growth of particles between transfer and cloud evacuation. A different explanation could be that larger heptadecane particles were present (as larger dust particles in the dust experiment) before the evacuation started. Such particles could have swollen or already activated into cloud particles. The SMPS size distributions only extend to 615nm, thus, we cannot say whether larger particles were indeed present. Another explanation that cannot be ruled out completely is, that other aerosol particles from background contamination are activated

25 and cause the first activation mode. However, it is not clear why contamination should only be existent in the heptadecane experiments and not in the α-pinene and TMB experiments as well.

As Mikhailov et al. (2009) point out, organic (semi-)solid amorphous particles can kinetically limit the water uptake and may thus influence the growth activation as cloud condensation nuclei. Thus, the phase state of the aerosol particles (represented by their bounciness) could play a role in the onset of activation. As the cloud chamber is generally at about water saturation

30 at the beginning of each expansion, an earlier activation to cloud particles would be expected than seen here. It is likely, that the observation of cloud particles is delayed due to wall heating effects, i.e. the cloud forms in the middle of the chamber but when starting sucking air into the sample lines to the cloud particle instrumentation, air from the boundary layer between wall and chamber interior is drawn into the lines first which might be at slightly higher temperatures and therefore at lower relative humidity and cloud free. Such wall effects have been observed in other cloud chambers as the AIDA chamber as well

35 (Möhler et al., 2003).

The comparison of activated fractions shows some differences between the investigated aerosol particles: while most experiments show no or only little signs of cloud processing in terms of a changed activated fraction of aerosol particles to cloud particles, TMB activated fractions in the second run are lower than in the first run. Thus, after the first cloud cycle the TMB particles are less likely to form cloud droplets, though the mean mode diameter shifted slightly to larger sizes which should

5   foster faster droplet activation. α-pinene shows a similar behaviour, though less obvious. Generally, cloud processing is thought to increase the efficiency of activation into cloud particles (e.g. Hoose et al., 2008). However, as the experiments reported here exhibit pure SOA aerosol, and we expect no other organic and inorganic material (or vapours) in the chambers, cloud processing here will only change the aerosol mass, not aerosol chemistry. Only remaining organic vapour can condense into the droplets. Uptake of organic vapours during the first cloud cycle and thus, less vapour available during the second cloud cycle

10 could lead to a smaller effect of co-condensation (Topping et al., 2013) and thus, smaller cloud particle numbers and reduced activated fractions. Dust as well showed a higher activated fraction during the first run, however, one has to bear in mind the higher pump speed used in that run. Heptadecane shows a contrary behaviour to the other SOA compounds: In the slow pump speed experiment, the second cloud cycle exhibits higher activated fractions than the first cycle with numbers comparable to those in the cloud cycles of the fast pump speed experiment. In the latter no significant difference in activated fractions between

15 the two cloud runs can be distinguished. It has to be noted that the mean mode diameter of the aerosol in the runs using the fast pump speed were about 400nm, but approximately 500nm in the slow runs. In general, the heptadecane runs show significantly smaller activated fractions than the runs using the bouncy compounds, even though the aerosol mean mode diameters are larger than in the TMB and α-pinene experiments.

A further small difference between the bouncy and non-bouncy compounds is the growth of particle sizes during cloud eva-

20 cuations: While in the heptadecane runs (non-bouncy) the MVD increases slightly with time, it stays fairly constant in the α-pinene and TMB runs. This might be due to the smaller activated fractions in the heptadecane experiments which leave more water vapour for further growth of the particles further into the cloud evacuation.

5   Conclusions

25 The coupled system of the Manchester Aerosol and Ice Cloud Chamber have been used to investigate the ice nucleating ability of SOA particles at temperatures resembling mixed-phase clouds. SOA particle were formed on precursors in the aerosol chamber by photo-oxidation. Clouds were formed by evacuation of the cloud chamber that led to a drop in temperature from approximately -20°C to about -28°C/-25.5°C (fast/slow pump speed, respectively) fostering cloud formation. At the start of the chamber evacuation the humidity inside the chamber was at about water saturation, allowing for a speedy onset of

30 cloud formation. The measurements show that the photo-oxidised SOA particles are no efficient ice nucleating particles in the tested temperature range: No ice formation was observed, irrespective of the type of SOA particles that were used (α-pinene, heptadecane, and TMB), resembling biogenic/anthropogenic and bouncy/non-bouncy compounds. A sensitivity experiment using kaolinite showed that ice formation was possible with the given setup.

While the bounciness (which basically represents the phase state) of the particles has no measurable impact on ice nucleation under the reported conditions, the SOA particles of different bounciness show differences in activation and cloud processing. TMB and α-pinene show reduced activated fractions in a subsequent cloud cycle, the less bouncy compound heptadecane reveals increased activated fractions. The exact reasons can only be speculated on as for example no measurements of organic
5 vapours in the chambers are available. Furthermore, heptadecane shows a two-fold cloud activation feature that is absent in the TMB and α-pinene experiments. Again, these cannot be fully explained here as measurements which would be able to support or disapprove the speculations are missing.

The main conclusions from these experiments are that the tested photo-oxidised SOA particles do not nucleate ice under the mixed-phase cloud regime. Thus, even in their high abundance in nature, SOA particles will rather act as cloud condensation
10 nuclei and only as ice nucleating particles when cold enough (below homogeneous freezing threshold).

6 Data availability

As the chambers are part of the EUROCHAMP consortium, the data will be made available at the EUROCHAMP data centre. Until then, they will be distributed upon request.

Appendix A: Temperature correction

15 During evacuations the temperature in the cloud chamber is supposed to be quasi-adiabatic, if no clouds form. By considering the time constant, a quasi-adiabatic temperature drop can be seen at the beginning of the expansion, while heating effects become stronger later on from wall heating and latent heat release from droplet formation. Fig. A1 shows the temperatures during a cloud expansion (in the lower panel): measured temperature in red, calculated adiabatic temperature in blue, and the corrected temperature considering the time constant in orange and dashed. The corrected temperature is smoothed with a
20 20 seconds running mean due to the small scale fluctuations in the temperature measurements that otherwise propagate into the corrected temperature. Additionally, the plot shows the pressure. In the upper panel the measured cloud particle number concentrations are displayed in green triangles. They give a good indication for the bump in the corrected temperature at 20 seconds, as the major activation (sharp increase in particle numbers) coincides with the temperature deviation. By calculating the theoretically available humidity from these retrieved temperatures we find a good match with our LWC observations, as the
25 calculated available LWCs in the upper panel show.

Author contributions. WF and DH main measurements operations and (preliminary - DH) data analysis, with help of JD and RA. Concept GM and PC. WF main writing. All contributed to discussions and fine tuning of manuscript.

Competing interests. The authors declare no competing interests.

Acknowledgements. The authors like to thank Lee Paul and Barry Gale for technical help with the chambers and the air system. The experiments reported in this manuscript were carried out in the project CCN-Vol_IN_Bounce that was funded by the Natural Environment Research Council (NERC) under the grant code NE/L007827/1. PC acknowledges funding from the European Union's 7th Framework Programme BACCHUS (FP7/2007-2013) under grant agreement number 603445.

5 References

Adler, G., Haspel, C., Moise, T., and Rudich, Y.: Optical extinction of highly porous aerosol following atmospheric freeze drying, J. Geophys. Res. Atmos., pp. 2013JD021 314–, http://dx.doi.org/10.1002/2013JD021314, 2014.

Alfarra, M. R., Good, N., Wyche, K. P., Hamilton, J. F., Monks, P. S., Lewis, A. C., and McFiggans, G.: Water uptake is independent of the inferred composition of secondary aerosols derived from multiple biogenic VOCs, Atmospheric Chemistry and Physics, 13, 11 769–
5   11 789, doi:10.5194/acp-13-11769-2013, http://www.atmos-chem-phys.net/13/11769/2013/, 2013.

Connolly, P. J., Flynn, M. J., Ulanowski, Z., Choularton, T. W., Gallagher, M. W., and Bower, K. N.: Calibration of the Cloud Particle Imager Probes Using Calibration Beads and Ice Crystal Analogs: The Depth of Field, Journal of Atmospheric and Oceanic Technology, 24, 1860–1879, http://dx.doi.org/10.1175%2FJTECH2096.1, 2007.

Connolly, P. J., Emersic, C., and Field, P. R.: A laboratory investigation into the aggregation efficiency of small ice crystals, Atmospheric
10   Chemistry and Physics, 12, 2055–2076, doi:10.5194/acp-12-2055-2012, http://www.atmos-chem-phys.net/12/2055/2012/, 2012.

Dye, J. E. and Baumgardner, D.: Evaluation of the Forward Scattering Spectrometer Probe. Part I: Electronic and Optical Studies, Journal of Atmospheric and Oceanic Technology, 1, 329–344, 1984.

Emersic, C., Connolly, P. J., Boult, S., Campana, M., and Li, Z.: Investigating the discrepancy between wet-suspension- and dry-dispersion-derived ice nucleation efficiency of mineral particles, Atmospheric Chemistry and Physics, 15, 11 311–11 326,
15   doi:10.5194/acp-15-11311-2015, http://www.atmos-chem-phys.net/15/11311/2015/, 2015.

Hamilton, J. F., Rami Alfarra, M., Wyche, K. P., Ward, M. W., Lewis, A. C., McFiggans, G. B., Good, N., Monks, P. S., Carr, T., White, I. R., and Purvis, R. M.: Investigating the use of secondary organic aerosol as seed particles in simulation chamber experiments, Atmospheric Chemistry and Physics, 11, 5917–5929, doi:10.5194/acp-11-5917-2011, https://www.atmos-chem-phys.net/11/5917/2011/, 2011.

Hoose, C. and Möhler, O.: Heterogeneous ice nucleation on atmospheric aerosols: a review of results from laboratory experiments, Atmos-
20   heric Chemistry and Physics, 12, 9817–9854, doi:10.5194/acp-12-9817-2012, https://www.atmos-chem-phys.net/12/9817/2012/, 2012.

Hoose, C., Lohmann, U., Bennartz, R., Croft, B., and Lesins, G.: Global simulations of aerosol processing in clouds, Atmospheric Chemistry and Physics, 8, 6939–6963, doi:10.5194/acp-8-6939-2008, https://www.atmos-chem-phys.net/8/6939/2008/, 2008.

Hoppel, W. A., Frick, G. M., Fitzgerald, J. W., and Larson, R. E.: Marine boundary layer measurements of new particle formation and the effects nonprecipitating clouds have on aerosol size distribution, Journal of Geophysical Research: Atmospheres, 99, 14 443–14 459,
25   doi:10.1029/94JD00797, http://dx.doi.org/10.1029/94JD00797, 1994.

Koop, T., Bookhold, J., Shiraiwa, M., and Poschl, U.: Glass transition and phase state of organic compounds: dependency on molecular properties and implications for secondary organic aerosols in the atmosphere, Phys. Chem. Chem. Phys., 13, 19 238–19 255, doi:10.1039/C1CP22617G, http://dx.doi.org/10.1039/C1CP22617G, 2011.

Mikhailov, E., Vlasenko, S., Martin, S. T., Koop, T., and Pöschl, U.: Amorphous and crystalline aerosol particles interacting with water vapor:
30   conceptual framework and experimental evidence for restructuring, phase transitions and kinetic limitations, Atmospheric Chemistry and Physics, 9, 9491–9522, doi:10.5194/acp-9-9491-2009, https://www.atmos-chem-phys.net/9/9491/2009/, 2009.

Möhler, O., Stetzer, O., Schaefers, S., Linke, C., Schnaiter, M., Tiede, R., Saathoff, H., Krämer, M., Mangold, A., Budz, P., Zink, P., Schreiner, J., Mauersberger, K., Haag, W., Kärcher, B., and Schurath, U.: Experimental investigation of homogeneous freezing of sulphuric acid particles in the aerosol chamber AIDA, Atmospheric Chemistry and Physics, 3, 211–223, doi:10.5194/acp-3-211-2003,
35   https://www.atmos-chem-phys.net/3/211/2003/, 2003.

Murray, B. J., Wilson, T. W., Dobbie, S., Cui, Z., Al-Jumur, S. M. R. K., Mohler, O., Schnaiter, M., Wagner, R., Benz, S., Niemand, M., Saathoff, H., Ebert, V., Wagner, S., and Karcher, B.: Heterogeneous nucleation of ice particles on glassy aerosols under cirrus conditions, Nature Geosci, 3, 233–237, http://dx.doi.org/10.1038/ngeo817, 2010.

Prenni, A. J., Petters, M. D., Faulhaber, A., Carrico, C. M., Ziemann, P. J., Kreidenweis, S. M., and DeMott, P. J.: Heterogeneous ice nucleation measurements of secondary organic aerosol generated from ozonolysis of alkenes, Geophysical Research Letters, 36, n/a–n/a, doi:10.1029/2008GL036957, http://dx.doi.org/10.1029/2008GL036957, l06808, 2009.

Pruppacher, H. R. and Klett, J. D.: Microphysics of Clouds and Precipitation, vol. 18 of *Atmospheric and Oceanographic Science Library*, Kluwer Academic Publishers, 2 edn., 1997.

Shiraiwa, M., Li, Y., Tsimpidi, A. P., Karydis, V. A., Berkemeier, T., Pandis, S. N., Lelieveld, J., Koop, T., and Pöschl, U.: Global distribution of particle phase state in atmospheric secondary organic aerosols, Nature Communications, 8, 15 002, http://dx.doi.org/10.1038/ncomms15002, 2017.

Topping, D., Connolly, P., and McFiggans, G.: Cloud droplet number enhanced by co-condensation of organic vapours, Nature Geosci, 6, 443–446, http://dx.doi.org/10.1038/ngeo1809, 2013.

Virtanen, A., Joutsensaari, J., Koop, T., Kannosto, J., Yli-Pirila, P., Leskinen, J., Makela, J. M., Holopainen, J. K., Poschl, U., Kulmala, M., Worsnop, D. R., and Laaksonen, A.: An amorphous solid state of biogenic secondary organic aerosol particles, Nature, 467, 824–827, http://dx.doi.org/10.1038/nature09455, 2010.
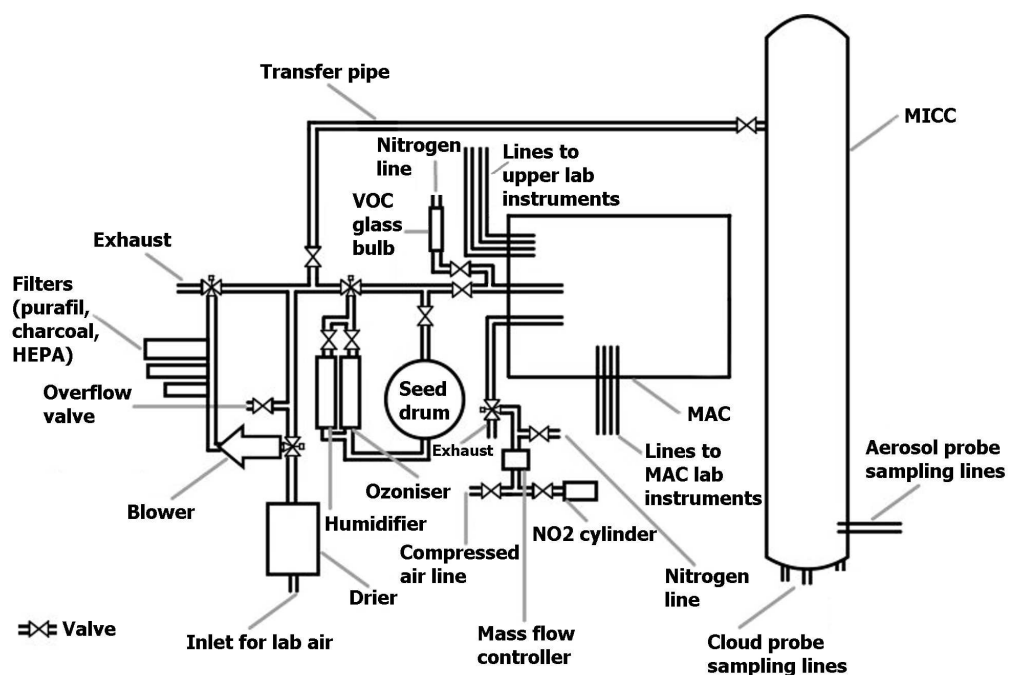
Figure 1. Drawing of the aerosol (MAC) and cloud (MICC) chambers, air system, connecting pipes, and various sampling lines.
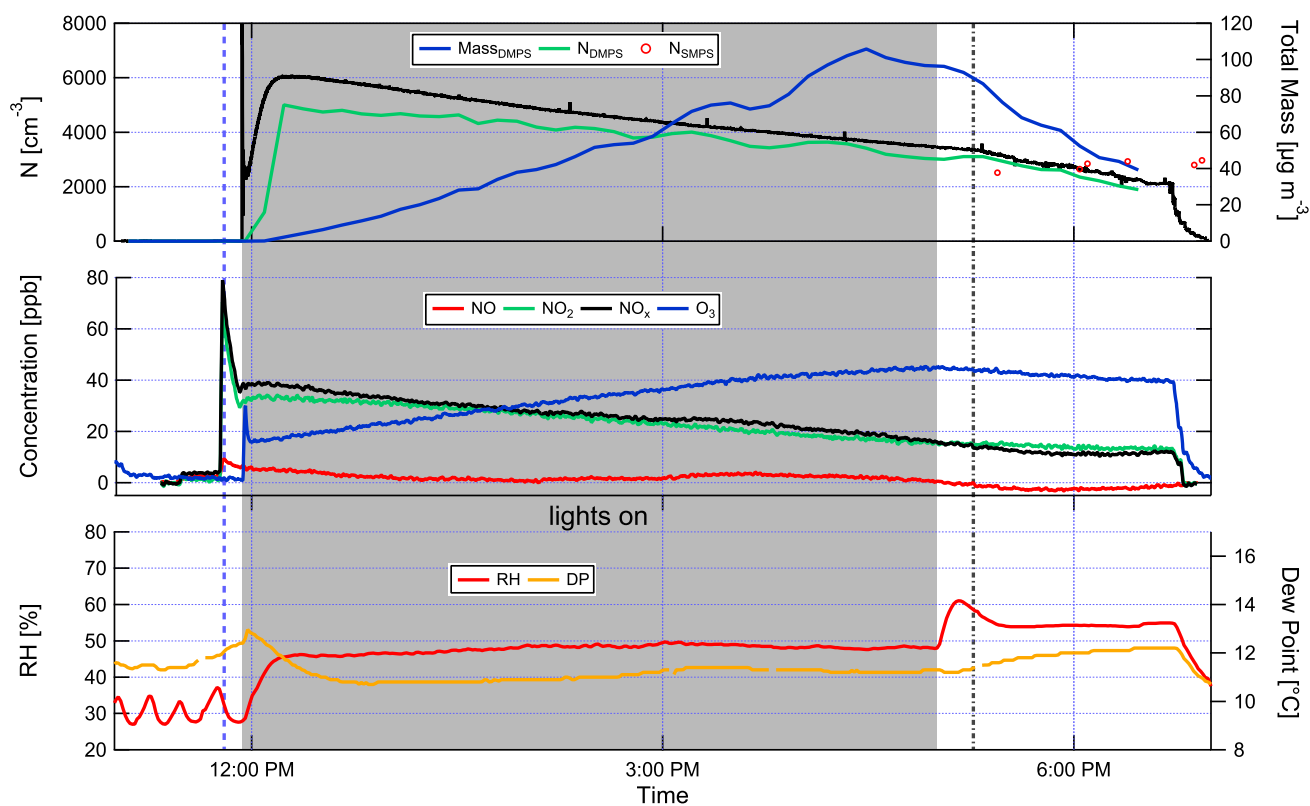
Figure 2. Development of SOA particles in the aerosol chamber. The blue dashed line indicates the injection of the SOA precursors, the grey dash-dotted line the beginning of the transfer to the cloud chamber. The grey shading indicates the time with the lights switched on.
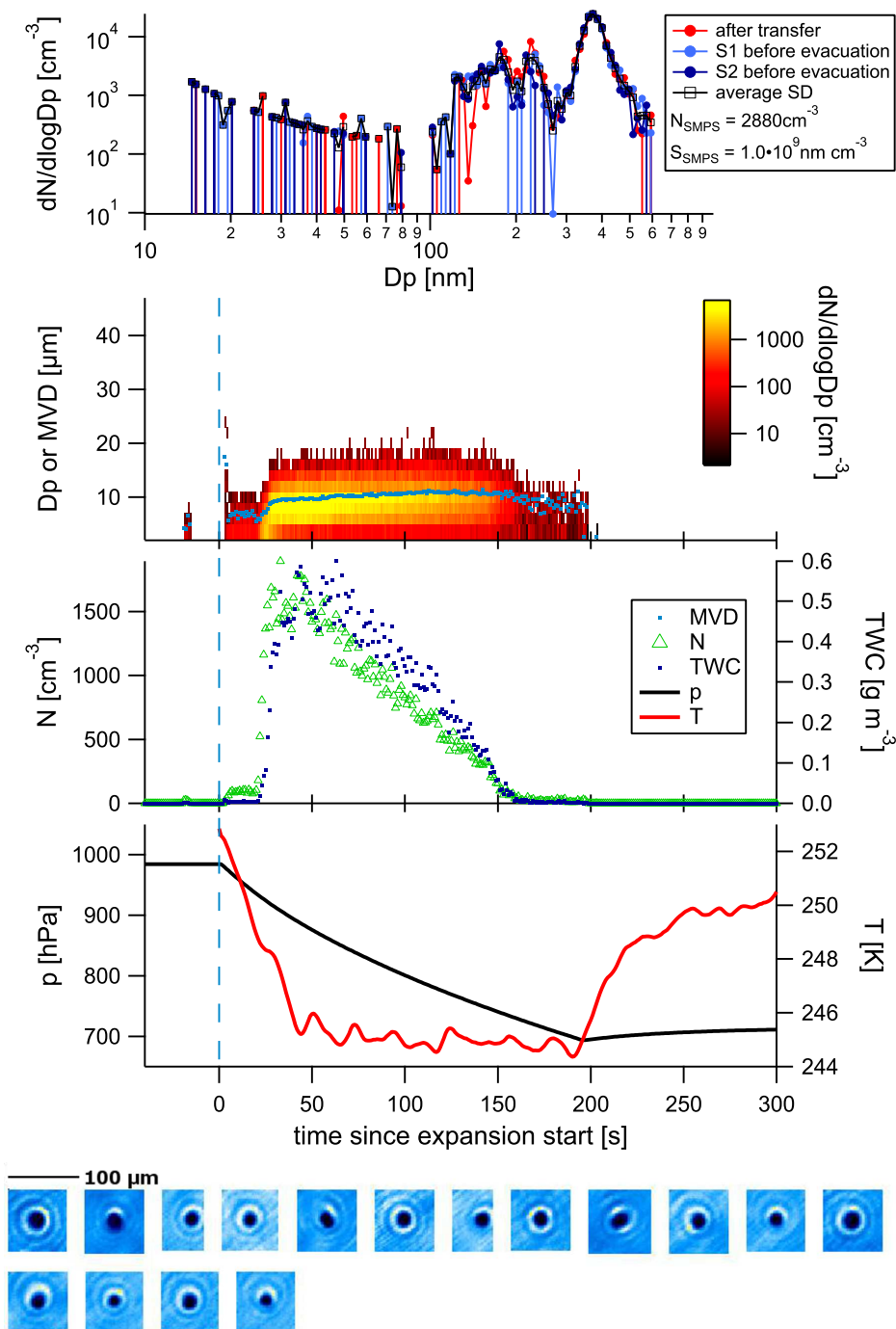
Figure 3. Example of a cloud evacuation performed on heptadecane precursor aerosol. The uppermost panel shows the SMPS size distributions obtained before the expansion, followed by timeseries of FSSP measurements, size distribution and mean volume diameter (MVD, panel b), total water content (TWC) and number concentration (N, panel c), and temperature and pressure (panel d) during evacuation. This was the second run on the aerosol population with a fast pump speed.
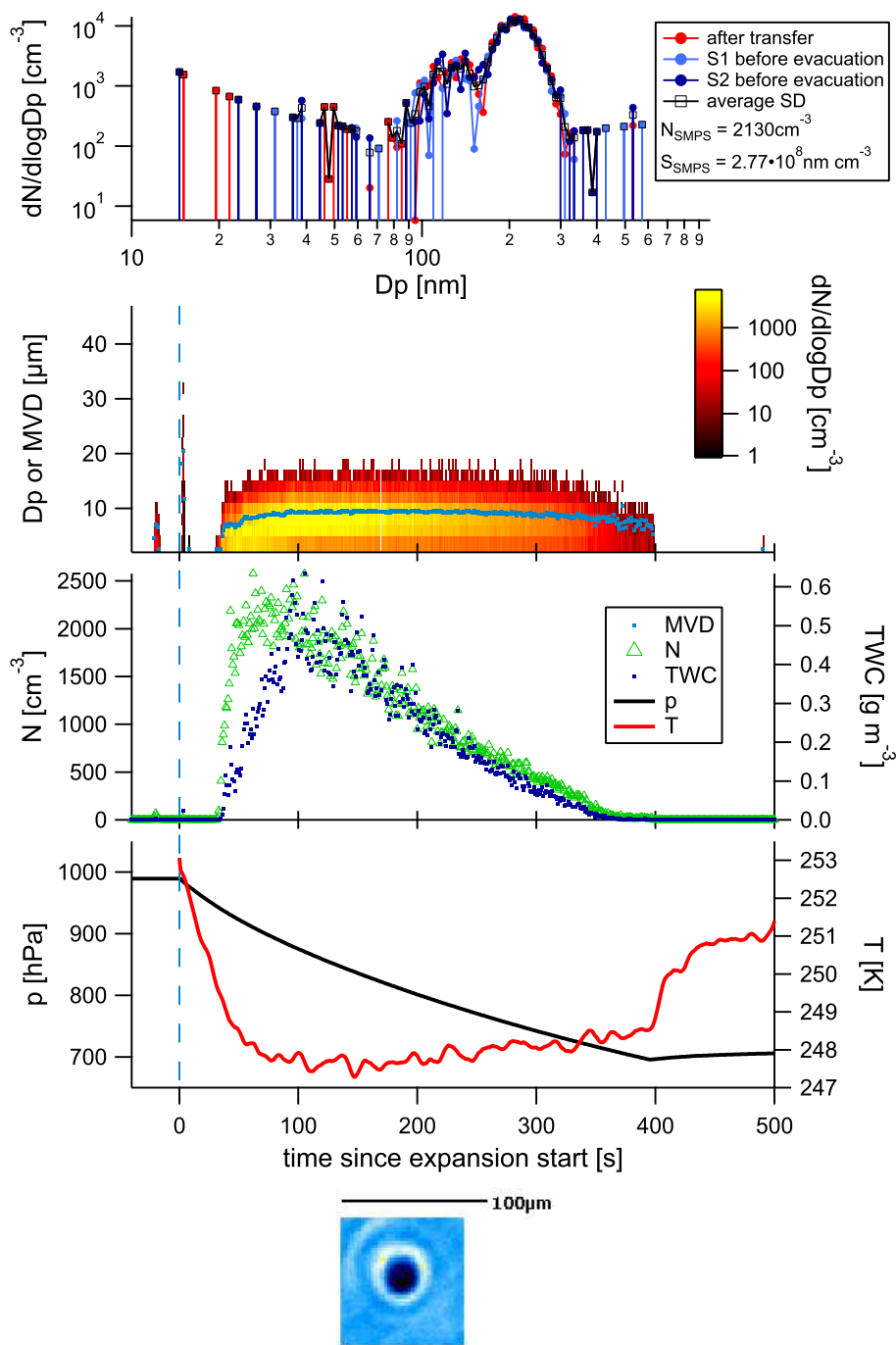
Figure 4. As Fig. 3 but using α-pinene as SOA precursor. This evacuation was the second run on the aerosol population, performed with a slow pump speed. Only one image was sampled by the CPI.
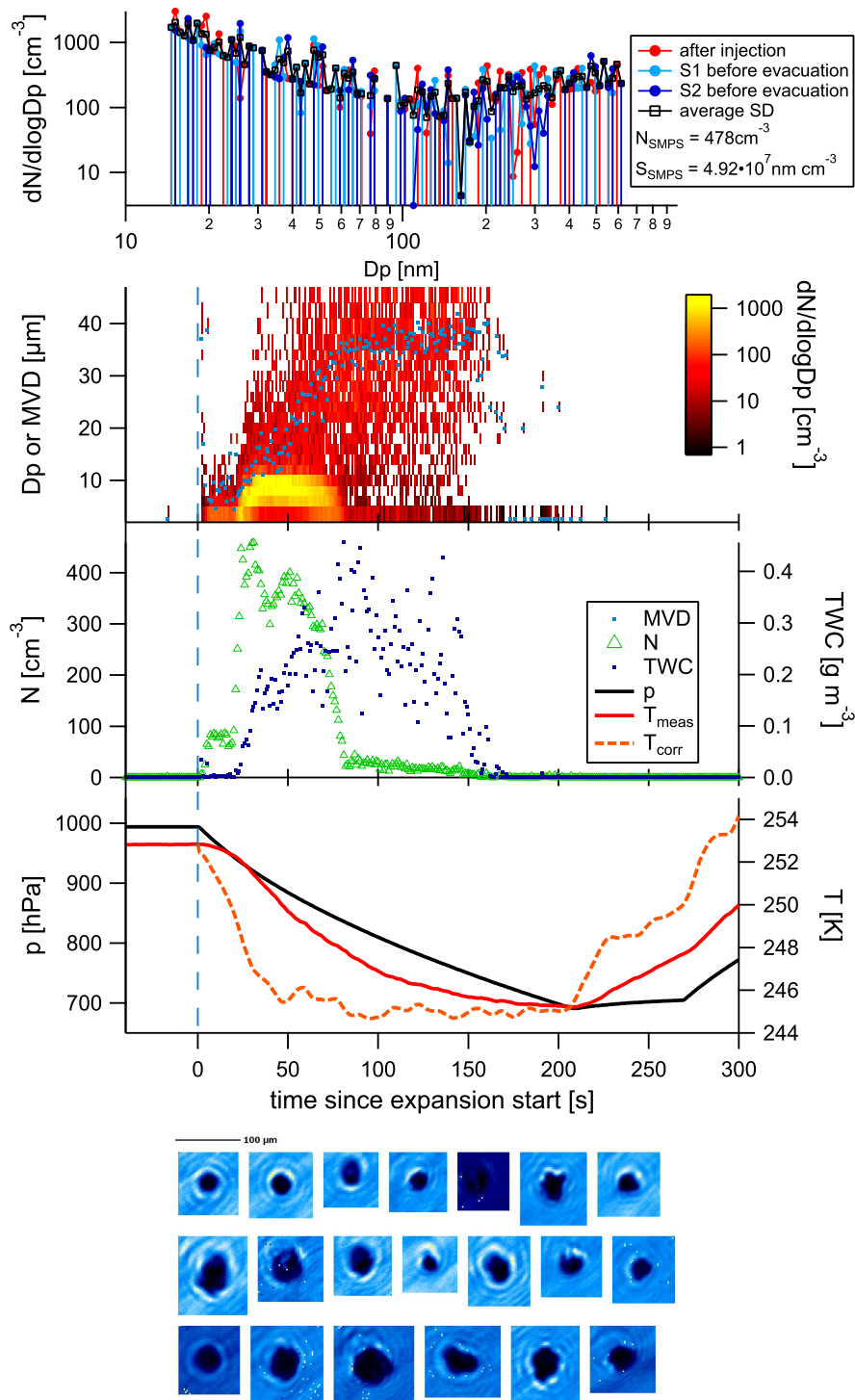
Figure 5. Control experiment using dust. Panels as in Fig. 3, the data shown here stem from the first run, using a high pump speed. The data show formation of ice in a second mode and the eating up of smaller drops over time.
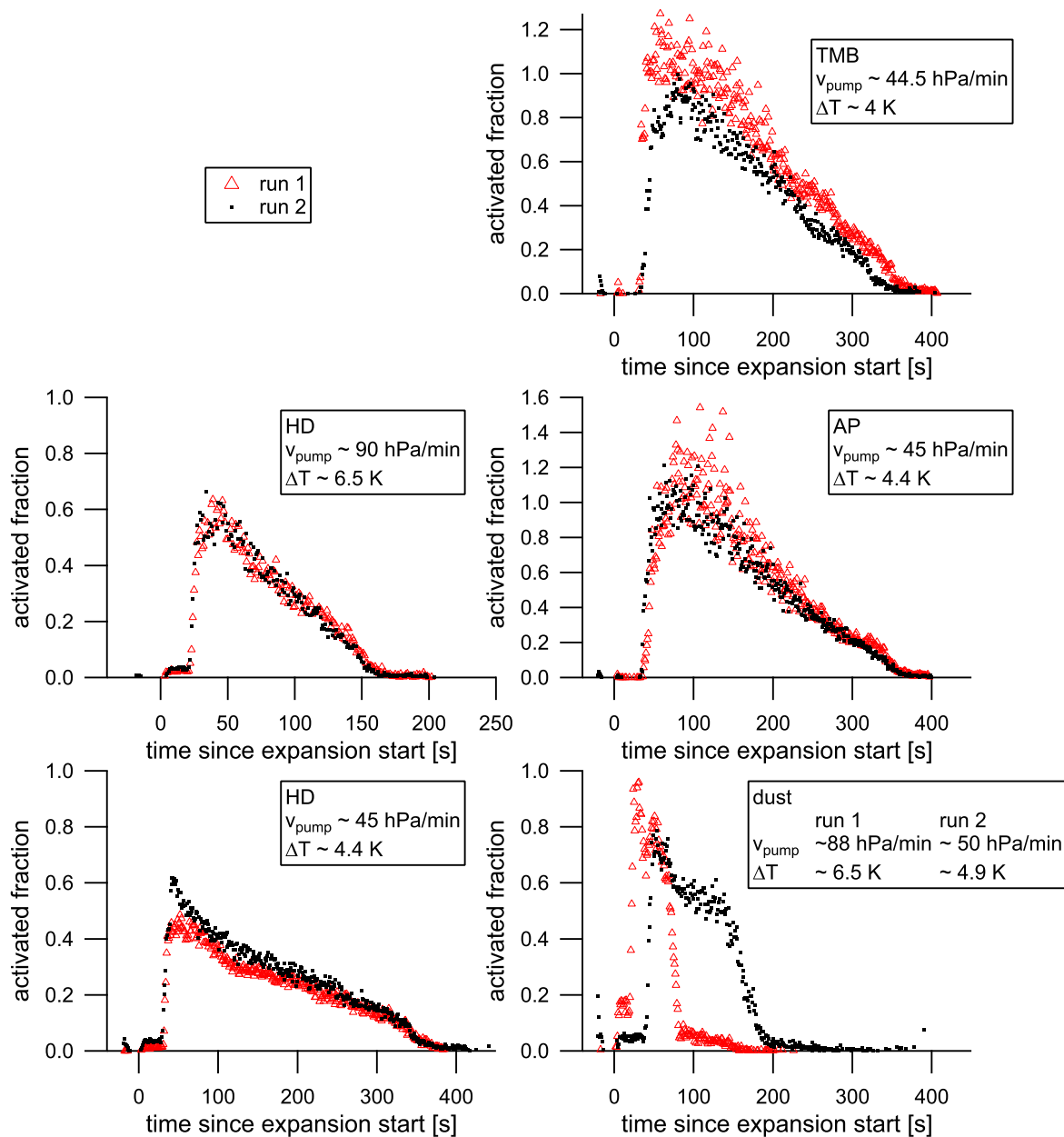
Figure 6. Activated fractions of aerosol to cloud particles for heptadecane (HD; left hand side), TMB (TMB; upper right), α-pinene (AP; middle right), and dust (lower right). The first cloud evacuation run is shown by the red triangles, the second run by black dots. Pump speed and temperature drop during evacuation are given in the legends.
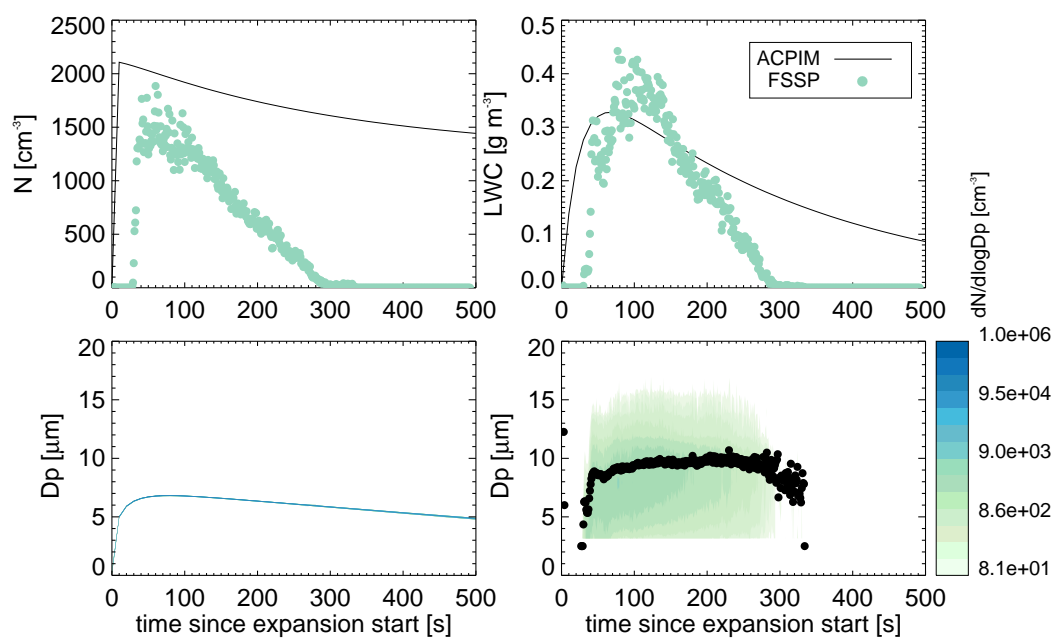
Figure 7. Comparison of ammonium sulfate measurements and ACPIM simulation of number concentrations (upper left), LWC (upper right), size distribution and mean volume diameter (lower panels, measured right, simulated left).

Table 1. Overview about the conducted experiments, indicating pump speeds, number of cloud runs performed, and times of cloud droplet activation in seconds from start of cloud expansion for first/second(/third) cloud run.

	system	pump speed	# runs	onset of main activation
Exp 1	clean	fast	3	23s/19s/19s
Exp 2	ammonium sulfate	fast	3	21s/16s/18s
Exp 3	SOA background	fast	2	19s/20s
Exp 4	α-pinene	fast	2	19s/24s
Exp 5	SOA background	fast	2	19s/20s
Exp 6	heptadecane	slow	2	31s/29s
Exp 7	TMB	slow	2	34s/32s
Exp 8	α-pinene	slow	2	35s/30s
Exp 9	ammonium sulfate	slow	2	29s/27s
Exp 10	heptadecane	fast	2	21s/21s
Exp 11	dust (kaolinite)	fast and slow	2	21s/39s

Table 2. Initial nominal conditions for SOA formation in the aerosol chamber.

Experiment	precursor	amount injected	initial conditions after injection				
		(µl)	NO_x	O_3	VOC/NO_x	$Conc_{CPC}$ (cm^{-3})	$Mass_{SMPS}$ (μgm^{-3})
Exp 1	clean	-	-	-	-	-	<1
Exp 2	ammonium sulfate	for 60sec	9.8	1.2	-	8477/4288	0.824
Exp 3	SOA background	-	50.3	5.8	-	1.9	7.8e-5
Exp 4	α-pinene	29.72	38.9	10.3	6.4	25173	16.2
Exp 5	SOA background	-	43.2	13.8	-	3087	0.026
Exp 6	heptadecane	116	32.9	32.1	15.2	4289	4.2
Exp 7	TMB	52.2	55.0	21.7	9.1	4595	0.042
Exp 8	α-pinene	11.9	24.0	1.7	4.2	9990	4.3
Exp 9	ammonium sulfate	for 30sec	5.4	0.1	-	4824	0.719
Exp 10	heptadecane	116	38.8	16.2	12.9	6035	2.2
Exp 11	dust (kaolinite)			not filled via MAC			

6000

Table 3. Conditions in the aerosol chamber shortly before transfer to the cloud chamber and aerosol properties after transfer in MICC.

Experiment	precursor	time lights on [h]	NO [ppb]	NO$_2$ [ppb]	O$_3$ [ppb]	Conc$_{CPC}$ [cm^{-3}]	Mass$_{DMPS}$ [µgm^{-3}]	Conc$_{SMPS}$ [cm^{-3}]	Mass$_{SMPS}$ [µgm^{-3}]
						conditions at transfer in MAC		conditions after transfer in MICC	
Exp 1	clean	-	-	-	-	0.3	-	10.8$^!$	-
Exp 2	ammonium sulfate	-	9.2	0.3	0.7	3343	0.6	1993$^!$	-
Exp 3	SOA background	3:25	11.3	30.6	2.2	1.4	0.1	27.2$^!$	(<)
Exp 4	α-pinene	5:12	<	19.2	9.3	9255	83.9	8483	92.1
Exp 5	SOA background	5:36	1.0	25.5	17.8	1190	0.4	1082	0.6
Exp 6	heptadecane	5:34	<	8.4	54.9	2143	112.6	2021	95.4
Exp 7	TMB	5:47	3.1	34.1	36.4	1730	3.8	1737	8.4
Exp 8	α-pinene	5:30	<	9.7	9.8	2787	10.4	2817	14.9
Exp 9	ammonium sulfate	-	9.2	1.7	1.5	2077	0.3	1996	0.5
Exp 10	heptadecane	5:04	<	15.6	43.5	3353	92.9	2495	70.1
Exp 11	dust (kaolinite)*	-	8.2	6.0	1.1	1.3	<*	554	4.57

$^!$ SMPS data not available (too low number concentrations) or faulty, concentrations taken from CPC

* dust injected into MICC directly

< below detection limit
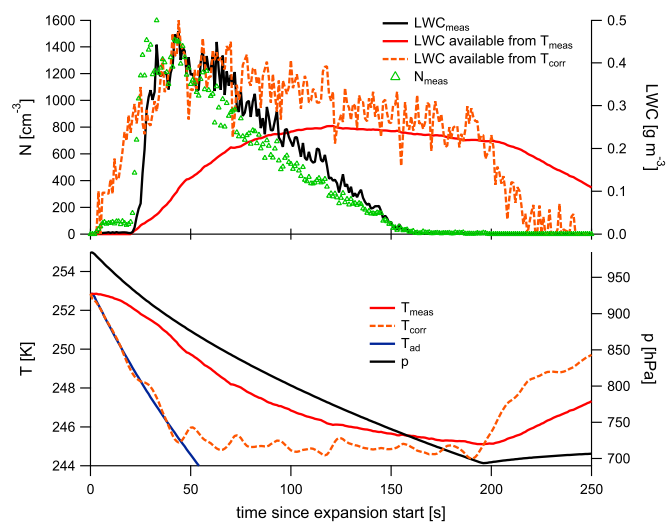
Figure A1. Measured and corrected temperatures and LWCs during the second heptadecane run. See text for details.